



# Simulation of Shock Propagation and Composite Fracture on a Pressure Vessel Composite Shell and Test Apparatus

Alexis Castel, Ph.D.<sup>1</sup> and Alain Trameçon.<sup>2</sup>

*ESI Group, Farmington Hills, MI, 48334, United States*

This paper presents an explicit finite element simulation model designed to analyze the behavior of structures under shock loads, including composite materials. The study introduces a methodology to precisely account for frictional losses at mechanical interfaces within the structure. Additionally, to illustrate the importance of friction, material damping is purposefully removed from the model. By accurately modeling friction, the simulation provides detailed insights into shock response dynamics and where non-linear dissipation occurs. Additionally, the model incorporates a standard failure criterion to evaluate the risk of composite fracture under extreme loading conditions. These findings contribute to the design and qualification assessment of aerospace components, offering a predictive framework ultimately reducing failure risks present in shock qualification testing.

## I. Nomenclature

$c_i$ , = the damping applied at a contact node  
 $k_i$ , = the stiffness penalty applied at a contact node,  
 $m_i$ , = the local mass associate with a contact node,  
 $x_i$ , = the local normal degree of freedom within a contact segment,  
 $\mu$  = constant friction coefficient  
 $t_N$ , = the normal force at a contact node  
 $t_T$ , = the tangential (traction) force at a contact node

## II. Introduction

In aerospace engineering, the ability to predict and mitigate shock-induced damage in composite materials is critical for ensuring the safety and reliability of spacecraft components under extreme conditions. Despite advances in shock analysis techniques, existing empirical models often fail to account for amplification effects and complex interactions in composite structures, potentially underestimating failure risks. Additionally, accurately capturing shock propagation requires precise modeling of interactions at structural interfaces and accounting for various energy losses, including those from structural damping and material properties. Furthermore, developing a reliable composite fracture model is essential for accurately predicting structural damage under shock loading conditions.

In this study, we employ a multi-purpose explicit finite element model (ESI's Virtual Performance Solution) to simulate a comprehensive shock test conducted at NASA's Jet Propulsion Laboratory (JPL) on a composite shell representative of a pressure vessel. While these tests were conducted independently at NASA JPL, this study aims to provide a simulation analysis of the results presented in [1]. This study reveals that amplification effects across structural joints can occur under shock loading, contradicting traditional attenuation assumptions and underscoring the need for more precise predictive methods.

<sup>1</sup> Technical Expert, Customer experience.

<sup>2</sup> Sr Manager, Product Management.

The simulation framework includes detailed modeling of the shock source, the test apparatus, and the fracture behavior of the composite shell. By integrating these elements, the simulation provides a holistic view of the shock response and fracture mechanisms.

This study advances shock response simulation by integrating detailed friction modeling at structural interfaces and isolating energy dissipation mechanisms, providing insights into composite fracture under shock loads. Due to data unavailability, the simulation predictions could not be validated against experimental results. The insights gained from this study contribute to a better understanding of shock propagation and fracture behavior in composite structures. This type of analysis is critical for the design and safety assessment of future aerospace components. This simulation approach offers additional insight into the structural dynamics of composite space systems early in the design phase, potentially leading to better-designed components and complete aerospace systems.

### III. Structure description

As described in [1], the structure studied in this paper comprises a composite shell designed to represent a quarter section of a pressure vessel supporting an imager used in a flight article at NASA's Jet Propulsion Laboratory (Figure 1). This was attached to a testing apparatus known as a tunable beam shock simulation system (TBSS), designed to meet a defined SRS spectrum through an impact test. The objective of this assembly is to capture interfaces and features of typical flight hardware so that shock transmission and potential failure modes can be studied.

The composite structure includes a plate mounted by struts that is a mass representation of the imager. Additionally, metallic boxes mounted to the top half of the composite shell serve as lumped masses totaling 250 lbs. to simulate the in-flight fluid loading on the flight pressure vessel (Figure 1). This introduces complexity as shock responses are affected by mass loading, which exhibit strong location- and frequency-dependent characteristics, as demonstrated in this recent experimental study. Shock tests were conducted with and without these masses to assess the effect of mass loading on the shell's shock behavior.

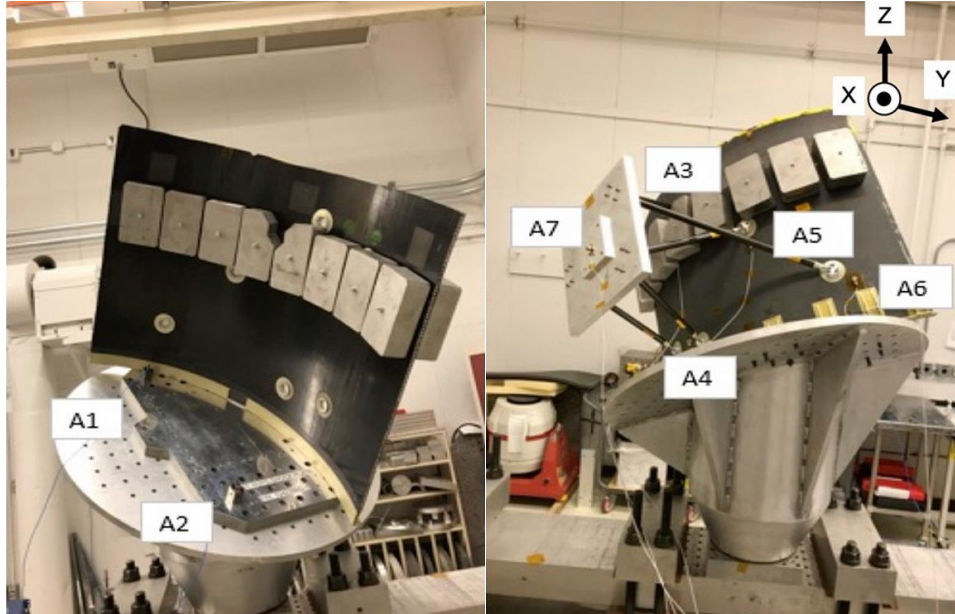


**Figure 1: Flight-representative composite structure with mounted hardware on the tunable beam shock test apparatus.**

To differentiate the composite modeling from the shock simulation, this paper will study the structure described above in two configurations:

- The test apparatus, comprising to the aluminum TBSS and its aluminum mounting system. The objective here is to study the shock simulation setup, the shock wave propagation and energy dissipation mechanisms.
- The complete model as described in the figure above. Here the objective is to study the behavior of the composite structure under a shock load.

#### IV. Finite element simulation setup

To account for the multiple complexities and nonlinearities of a transient shock model, we use an explicit finite element model due to its ability to handle the nonlinearity of materials and any slipping at the interface. The explicit formulation, with its typical very short time step, is suitable for shock simulations. The entirety of this study is conducted with ESI's Virtual Performance Solution (VPS). In order to avoid confusion in the different energy dissipation mechanisms, here, all solid elements were defined with selective reduced integration which do not exhibit any hourglass mode; therefore, this avoids any numerical dissipation associated to hourglass control in solid elements.

l.

The core concept of this model's setup is to distinguish between different energy dissipation mechanisms. Mainly, we aim here at distinguishing the energy being dissipated due to friction at the mechanical interfaces from the energy lost within the materials themselves. With this, we aim at accounting for both:

1. The very non-linear nature of energy losses within the structure. Indeed, due to the difference of static and dynamic friction coefficients, energy dissipation in contacts is non-linear by nature. This model aims at identifying and correctly capturing this effect.
2. The correct location of energy dissipation. Similarly, as opposed to a generic overall damping coefficient applied on the whole model, accurate modeling of contacts and dissipation mechanisms within the contacts allow for a more accurate spatial description of both the response and energy dissipation mechanisms.

##### A. Mechanical interfaces modeling overview

As the proposed model aims at accurately capturing the behavior of the shock response by representing losses due to friction at the interfaces, great care must be taken when choosing:

- A contact formulation
- A friction model
- Pre-loading contacts

To correctly present each of the above component, this section of the paper will focus on the support test structure as illustrated below:

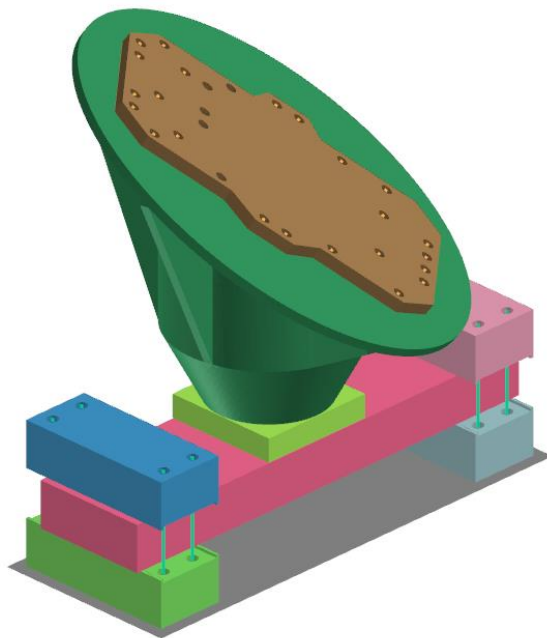


**Figure 2: Aluminum support structure for model description**

##### 1. Contacts formulation

The preliminary model used for this study leverages both symmetric and non-symmetric leader-follower node-to-segment/edge-oriented contact. This flexible formulation allows for different level of complexity in the parameters used for this study, limiting, when possible, the amount of information to characterize the contact to the minimum, in this case, a simple friction coefficient.

Contacts are enforced using a penalty method. Each contact is given a thickness and any slave node protruding within that thickness boundary is applied a resulting force based on a calculated stiffness.

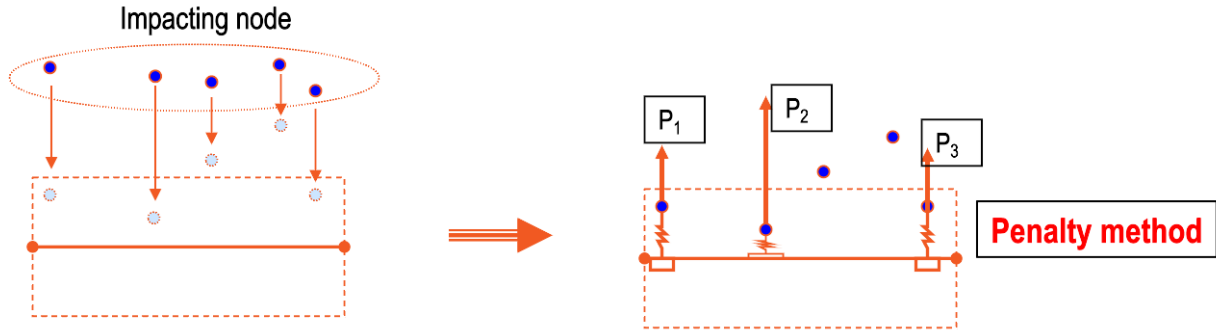


Figure 3: Contact penalty method representation

Here, the contact stiffness is evaluated for each contact pair from the material's properties, such as mass density and the speed of sound:

$$F_i = \text{SLFACM} \cdot \text{STF}(\text{SNODE}) \cdot p_i \quad (1)$$

where  $\text{STF}(\text{SNODE})$  is the mass-density/speed of sound based slave/master interaction stiffness. SLFACM here is a contact stiffness scale factor implemented to ensure the solution stability. This study uses the default value of SLFACM of 0.1.

Note that contact stiffness can be made non-linear to help with model stability. However, the specific model used in this study did not make use of non-linearity.

The penalty formulation acts as a spring element for modeling the contact with small penetrations. The penetrations are very small, and the associated contact elastic energy is negligible compared to the internal and friction energies.

## 2. Contact damping

Stiffness proportional damping internal to the contact is added to the normal penalty spring forces acting between the slave nodes and the master segments of this interface. Regarding the isolated action of the contact penalty spring,  $k_i$ , and of the added internal damper,  $c_i$ , on a slave node with mass,  $m_i$ , in the local normal degrees of freedom within a contact segment,  $x_i$ , the free vibration equation of motion becomes:

$$m_i \cdot \ddot{x}_i + c_i \cdot \dot{x}_i + k_i \cdot x_i = 0 \quad (2)$$

Although technically dissipative of energy, the purpose of the contact damping in this model is only to avoid sudden changes in contact forces from a time-step to another. Thus, for simplicity, the contact value is kept to a minimum value until contact forces do not vary sharply from one time step to another. Figure 4 shows the effect of contact damping during a loading phase on the contact force. In this case, the presence of damping in the contact formulation removes sharp variations in the contact forces.

By default, a 0.1 stiffness proportional damping factor to the local element critical damping is applied. The critical time step of the elements is in the range of 0.2  $\mu$ s, which leads to an average critical frequency of more than 1 MHz, well above the frequency range of the study.

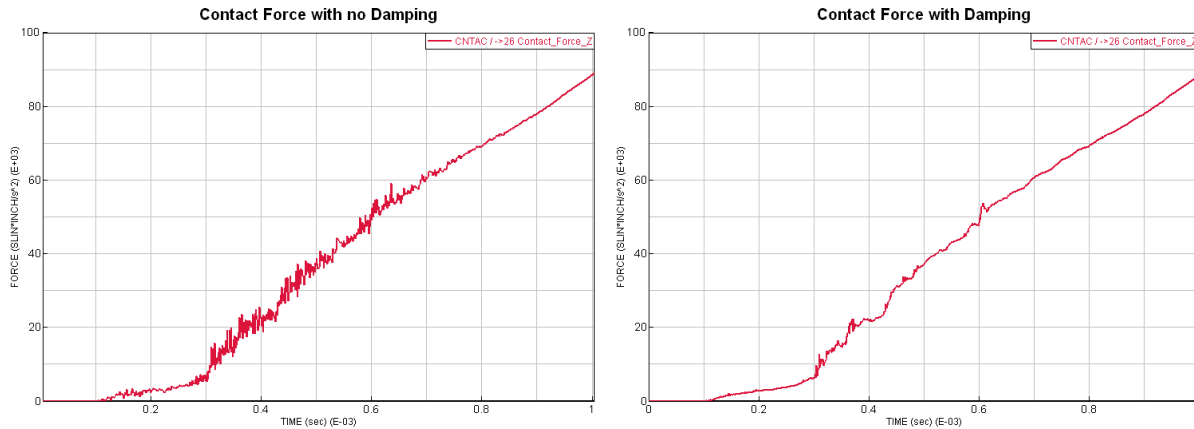


**Figure 4: Contact force with and without damping in the contact definition.**

### 3. Friction model

Although multiple friction models are available within the software, for this study, we are choosing a constant friction coefficient. Here, a constant coefficient arbitrarily chosen to be of  $\mu = 0.4$  as a reference value for aluminum on aluminum is set here. Therefore, we have the tangential (frictional) tractions  $t_T$  and normal force  $t_N$  between the slave and master surfaces satisfy the following:

$$\|t_T\| = 0.4 \cdot t_N \quad (3)$$

Note that, due to the nature of the contact formulation, a multitude of alternate friction models are available including models that are pressure dependent or velocity dependent (which would then capture the difference between static and dynamic friction coefficients). A combined pressure and velocity friction model where  $\mu = f(p) \cdot g(v)$  seems the most promising. However, given the context of this study and the lack of characterized joints, a constant friction coefficient is chosen.

### 4. Effect of pre-loading

A large part of correctly accounting for the friction between components is linked to the accurate representation of the static pre-loading due to bolts torque. To simplify the model setup, we choose to account for this pre-loading of the assembly during the first millisecond of the model simulation time. Bolt pre-load is applied as a linearly increased body force applied on each beam (representing a bolt). An arbitrary preload force of 4800 lbf set to be one fourth of the maximum load of a  $\frac{1}{2}$  in bolt was chosen. This value also guarantees that none of the model component meet a plastic strain. The following bolt pre-load table is then applied to all 43 bolts present in the model:

**Table 1: Bolt pre-load schedule**

Time (s)	Force (lbf)
0	0
0.001	4800
1	4800

The pre-load is applied over a millisecond and is modeled in an explicit analysis as a transient (dynamic) loading. In reality, the pre-load is an initial static condition and to represent this and to separate it from the following shock simulation, a temporary damping load is applied for the first 30 milliseconds of the simulation time. The overall objective is for the system to reach full equilibrium before any shock load is applied. For this, contact forces and overall model kinetic energy are monitored.

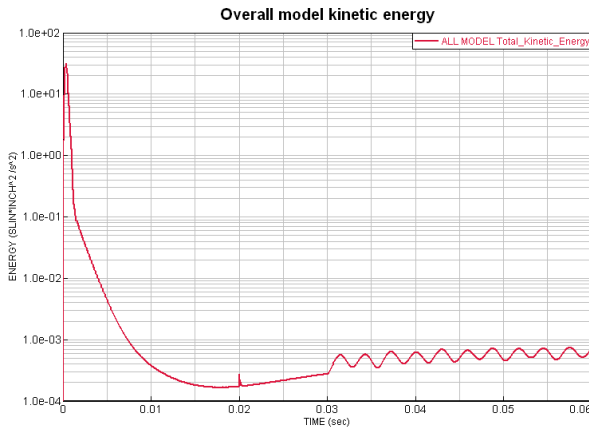


**Figure 5: Overall model kinetic energy vs time before shock load**

Figure 5Figure 1 shows the evolution of the model overall kinetic energy vs time, here, we clearly see the effect of the initial bolt load over the first millisecond, the effect of the damping load over the first 30 milliseconds and the system equilibrium, while never reaching a strict zero, the model here is considered stable and quasi static.

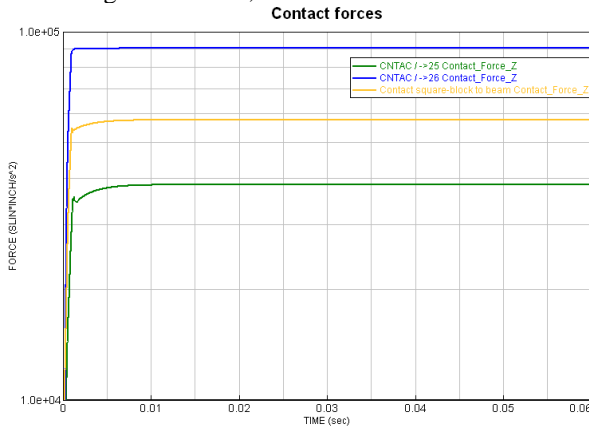


**Figure 6: Contact forces vs time before shock load**

Similarly, Figure 6 show the evolution of the contact forces vs time before shock load. Here, we are looking for stable contact forces before impact.

### B. Removing other sources of energy losses

So, to focus on evaluating losses due to friction, material losses are purposefully removed from the simulation model for the purpose of this study. It is worth noting that most of this model being made of aluminum, the intrinsic damping of aluminum is about 0.3% and therefore these losses should be considered neglectable. However, we could expect the composite shell added to the model later in this paper to add a more significant contribution to the material damping. Future model may include material damping as a function of the frequency. One of the noteworthy available material models is presented in [2].

Additionally, standard explicit models solved with Virtual Performance Solution make use of a Uniform Reduced Integration formulation on each element where hourglass damping is introduced into the model for stability. Here, to control where energy losses happen, this standard formulation was changed to Selected Reduced Integration, thereby removing other sources of damping. The main drawback of this approach is a moderate increase in solve time.

### C. Shock load and time domain calculation

The shock load is presented as a point force vs time applied over 4 nodes in the model at the base of the test apparatus as shown on Figure 7. The excitation corresponds to an impulse load starting at t=60 ms obtained from a modal hammer hit during a test performed at NASA JPL and part of the study presented in [1]. The amplitude of the impact force is shown on Figure 8Figure 10.

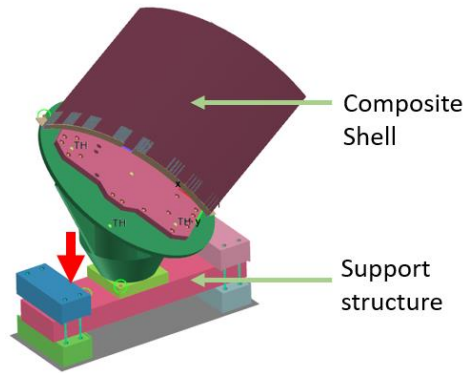


**Figure 7: Simulation setup with composite shell, showing the excitation locations (red arrow) and select data recovery locations (nodes noted TH and circled nodes)**

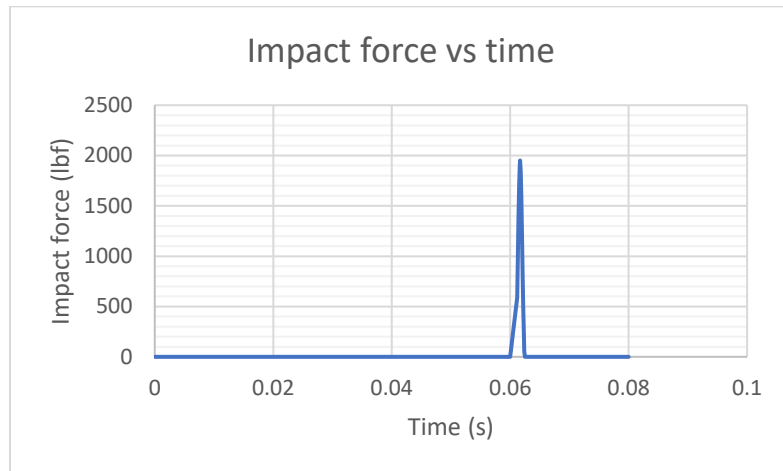


**Figure 8: Impact force vs time**

Following the impact load, the simulation is run up to  $t=0.5$ s so to observe the shock response in a transient manner until most of the initial energy is dissipated and Shock Response Spectra (SRS) can be calculated.

#### D. Fracture risk estimation

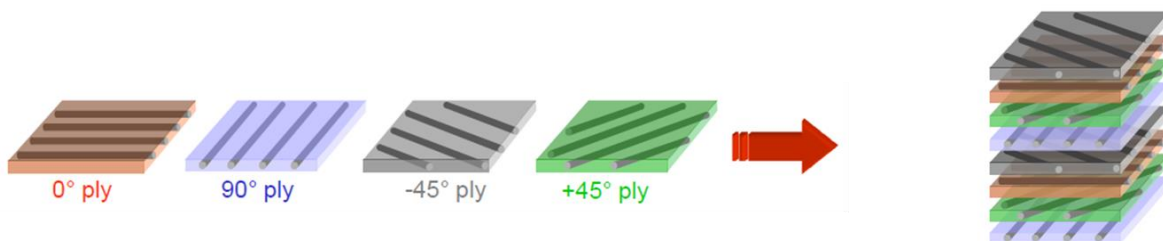


**Figure 9: example of a multilayered composite shell model**

Physical properties and thicknesses can be prescribed for each individual ply (or layer). Here, the physical properties are obtained from a direct translation of an implicit NASTRAN model. Then, to evaluate the fracture risk for each layer, a standard Tsai-Hill failure criterion is implemented, following the standard formulation:

$$f^2 = \sum_{i=1}^6 F_i \cdot \sigma_i + \sum_{i,j=1}^6 F_{ij} \cdot \sigma_i \cdot \sigma_j \quad (4)$$

The failure criterion here is determined by 13  $F_i$  and  $F_{ij}$  coefficients defined in [3].

The material properties of the imported model are augmented with generic failure criteria in traction and compression as shown in Table 2.

**Table 2: Carbon-Epoxy composite shell properties with failure criteria.**

Material	Carbon-Epoxy								
Density (lbf-s <sup>2</sup> /in <sup>4</sup> )	0.00015023								
Elastic Properties (psi)	E11	E22	E33	G12	G23	G13	nu12	nu23	nu13
	4.25E+07	8.10E+05	8.10E+05	5.60E+05	5.60E+05	5.60E+05	0.32	0	0
Traction failure (psi)	SIGtu11	SIGtu22	SIGtu33	TAUtu12	TAUtu23	TAUtu13			
	5.80E+04	2.90E+04	2.90E+04	3.50E+04	1.50E+04	3.50E+04			
Compression failure (psi)	SIGtu11	SIGtu22	SIGtu33	TAUtu12	TAUtu23	TAUtu13			
	5.80E+04	1.00E+06	1.00E+06	1.00E+06	1.00E+06	1.00E+06			

Failure is considered attained on a ply with  $f > 1$  for a ply of an element for more than 10 time steps. For this simulation, we chose to simply track failed element, however, one could opt to either update the material properties of a failed element or even to remove the element from the simulation to model the effects of the element failure.

## V. Shock simulation

This section aims at illustrating both the dissipation mechanisms in the shock model and the fracture modeling of the composite structure. As such, and to properly identify each phenomenon, multiple simulations of increasing complexity are run:

- A shock simulation with no composite structure where the only energy dissipation mechanism is due to the contact friction.
- A shock simulation where material damping (described **Error! Reference source not found.**) is introduced and added to the previous model
- A shock simulation where the composite structure is added to the test apparatus. Here, composite fracture risk is evaluated.

### A. Friction only simulation

This model description matches the illustration on Figure 2 as only the test apparatus support structure is present. Here, the model is set such that the only possible mechanism of energy dissipation is through friction work at the mechanical interface. Here the software can keep track of the energy dissipated in each contact as well as the energy stored as kinetic or elastic energy. In this model, we expect that most of the energy injected in the system during the shock excitation will be dissipated through energy losses in the contacts.

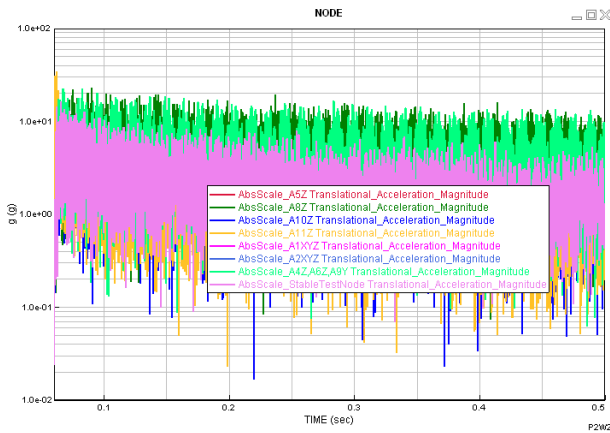
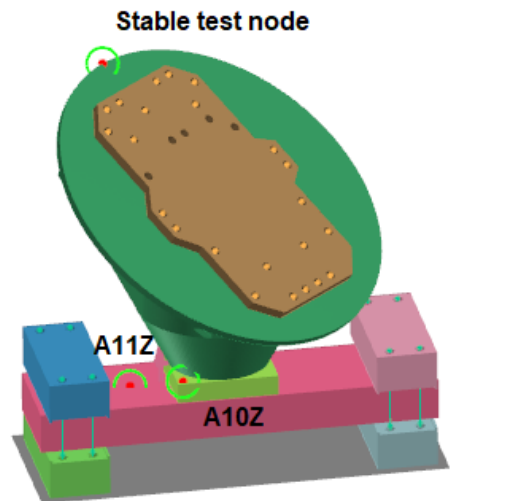


**Figure 10: Vibration response vs time on a log scale**

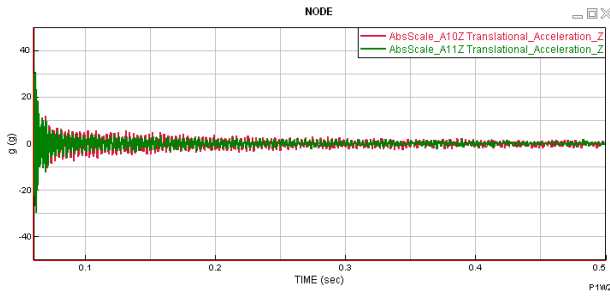
Figure 10 shows the vibration amplitude response vs time illustrating the energy dissipation mechanisms in the model. Here we see the amplitude of the vibration response ranging from 50g to about 10g after 0.5 seconds. Considering only part of the energy dissipation mechanisms are present in the model, this seems adequate for an initial simulation.

Figure 11 points out three specific recovery location on the initial model. Point A11Z is next to the hit point, point A10Z is located after one contact and the point named “Stable test node” is on top of the test apparatus. The three nodes identified time domain response is presented in Figure 12 and Figure 13. We see in the response vs time that the initial shock response is high at the beginning of the time history for point A11Z and quickly, the energy is distributed over the whole system. Interestingly, even on this simple example with no composite shell, the amplitude of the signal does not necessarily reduce with the number of interfaces. This is clearly shown on Figure 12 and Figure 13.

The SRS presented on Figure 14 illustrates the whole picture, where the initial impact is noted on the high frequency response of point A11Z and then the low frequency shows amplification for the point named “Stable test node”.



**Figure 11: 3 recovery point locations**



**Figure 12: Difference of response between impact point and after one interface**

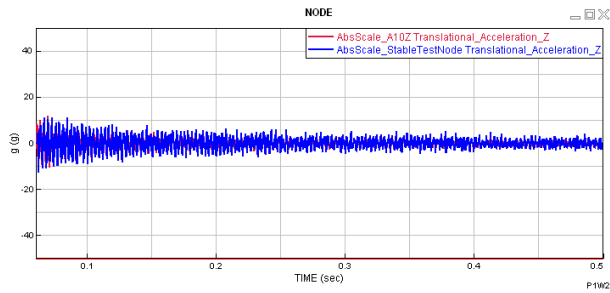


**Figure 13: Difference of response between second point and the recovery location named “Stable Test Node”**

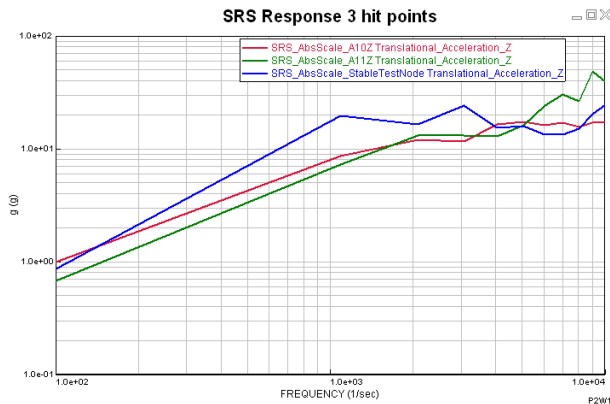


**Figure 14: Three monitor point SRS Response (Q=10)**

The energy response can also be monitored leading to an overview of both the stored and dissipated energy as shown on Figure 15. This figure plots the model internal energy (Kinetic + Elastic energy) was offset to a reference 0 at  $t=60$ ms to distinguish the energy variation observed during the shock simulation from the one observed during the pre-loading phase. This graph shows a large reduction of the internal energy of the model right after the initial impact, likely due to a slip of the preloaded structure, and then, we observe a transfer of the internal energy being dissipated through friction in the contact. The internal energy ends negative at the end of the simulation due to the offset and initial slip. Additionally, we can see here that the energy dissipated in the contact damping (as explained in IV-A-2), is negligible when compared to the energies involved in the shock simulation model.

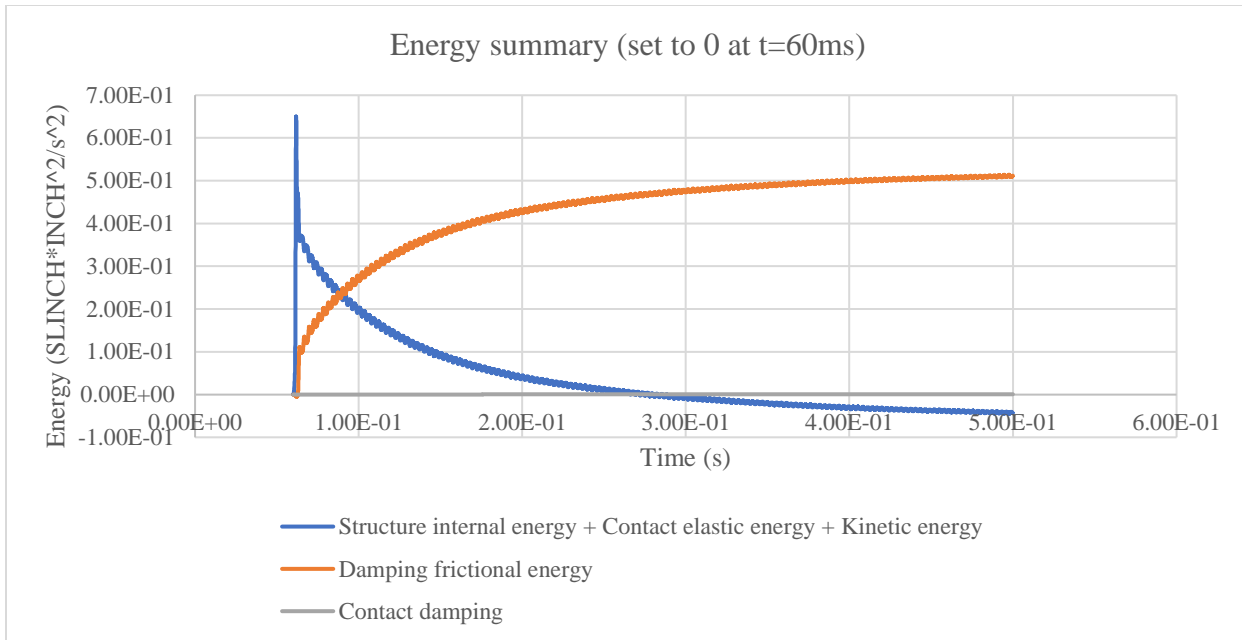


**Figure 15: Energy summary graph**

### B. Composite shell response and fracture estimation

To exacerbate the damage experienced by the composite shell, we decided to amplify the shock load by a factor 50 for illustrative purposes. The model is solved with the composite shell attached to the test structure using node-surface tied contacts, effectively connecting nodes (slaves) to surface (elements, 2D, 3D) withing a search box using a penalty method (as shown on Figure 16).

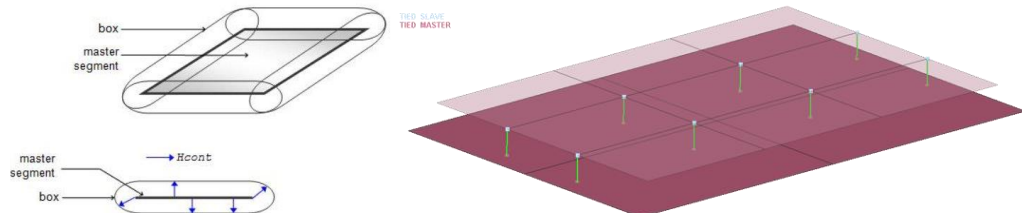


**Figure 16: Tied representation: search box on the left, projection of slave nodes on the master surface on the right.**

Four recovery points have been added to the model and the displacement and vibration response is recovered at these locations. The four points as well as the location of the tied contacts previously discussed are shown on Figure 17.

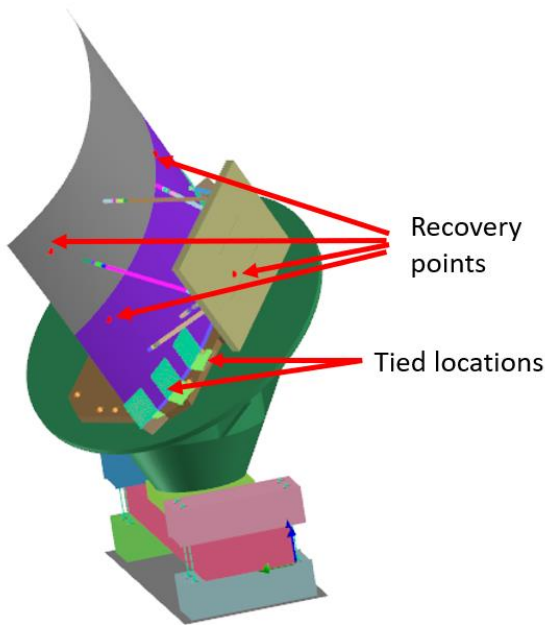


Figure 17: Recovery points and tied locations for the composite shell.

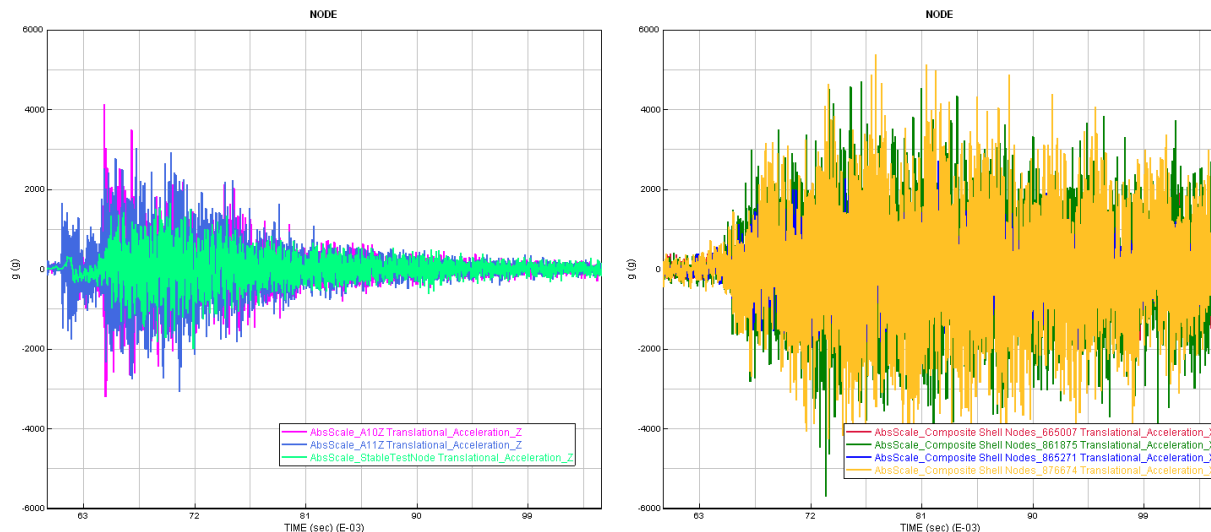


Figure 18: Time response of the monitor locations on support structure (left) and composite shell (right)

Figure 18 shows a clear amplification between the support structure and the composite shell as well as a delay of propagation of the initial shock wave. Figure 19 shows the corresponding SRS and does not show as clear of amplification pattern as what is shown in the time response. Indeed, out of the 4 randomly selected locations on the composite shells, 3 show amplification in the SRS while one shows lower levels. After verification, that lower level is also observed in the time domain data (Figure 18). Finally, Figure 20 shows the results of the composite failure criterion showing that for some locations, the composite plies failed (80% failure is the maximum possible as no failure criterion was applied to the face plies). The right side of the same figure shows in purple locations where at least one ply failed. The damage here was a bit exaggerated for illustrative purposes.

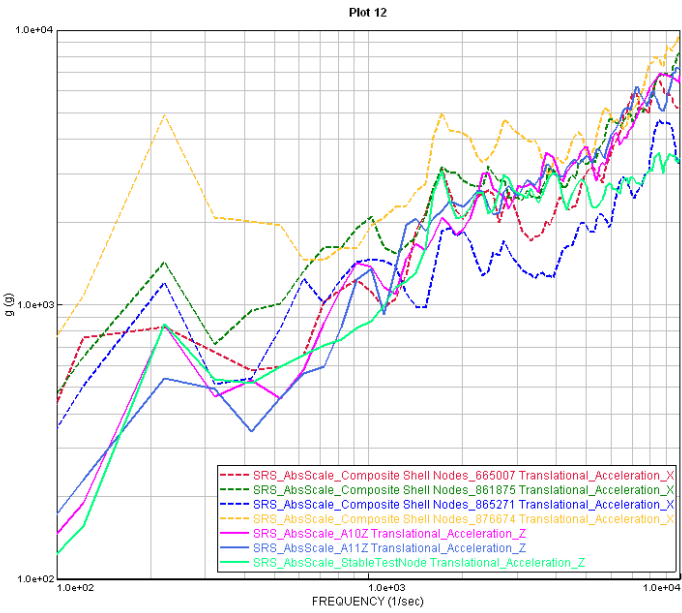


Figure 19: SRS response of the 7 monitored locations

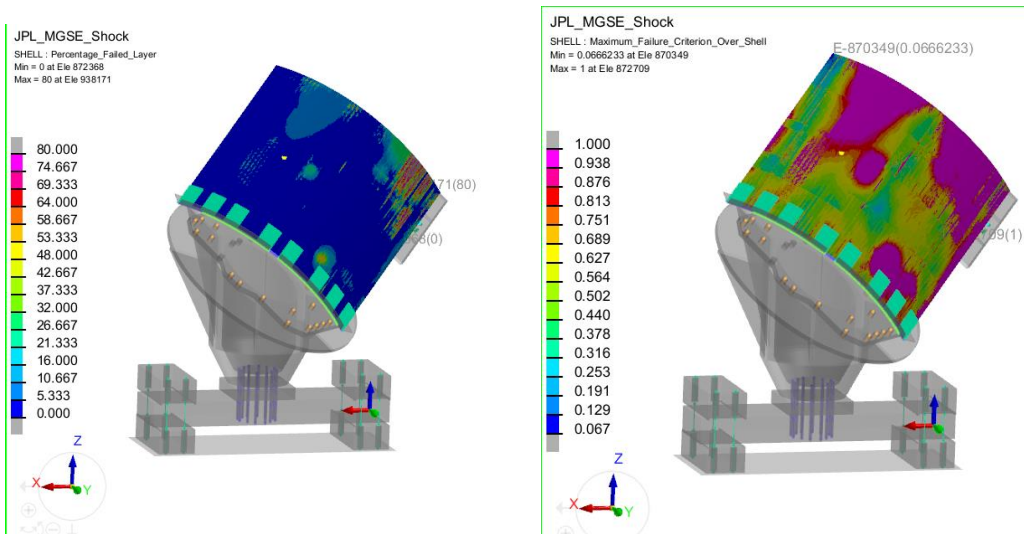


Figure 20: Composite shell percentage of failed layers (left) and maximum failure criterion over all layers (right)

## VI. Conclusions

This study developed and implemented a finite element simulation model to analyze the shock response and fracture behavior of a composite shell test apparatus under shock loading conditions. By leveraging an explicit finite element modeling approach, the study illustrates how transient shock events can be modeled, accounting for the non-linear energy dissipation mechanisms at mechanical interfaces. The explicit finite element formulation, with its fine time-step resolution, proved effective in addressing friction effects, providing detailed insights into the dynamic response of the structure. Additionally, intrinsic damping to material models can be accounted for with a dedicated material model such as the model described in [4].

The initial results from the explicit model demonstrated the ability to isolate frictional dissipation mechanisms and revealed amplification effects at structural joints, contradicting traditional assumptions of uniform attenuation. This capability highlights the importance of accurate friction modeling in assessing shock-induced energy transfer and

structural performance. Furthermore, the model's ability to clearly delineate energy dissipation pathways provides a valuable framework for understanding shock dynamics in aerospace applications.

Although experimental validation could not be conducted due to data unavailability, the initial results are promising. They underscore the utility of this approach for early-stage design assessments, offering critical insights into structural integrity and fracture risk under extreme loading conditions. This work contributes significantly to the predictive tools needed for designing and qualifying future aerospace systems, reducing failure risks, and enhancing overall reliability.

### Acknowledgments

The authors wish to acknowledge This work was done with the support of NASA JPL for the initial implicit model and feedback at the origin of this study.

### References

- [1] S. Pham and A. Kolaini, "Shock Model and Test Correlation for Structural Response Prediction," in *93rd Shock and Vibration Symposium*, Atlanta, GA, 2023.
- [2] A. M. S. a. T. A. Castel, "Fairing separation shock source evaluation and propagation," in *ECSSMET 2023*, Toulouse, France, 2023.
- [3] S. Tsai and E. Wu, "A General Theory of Strength for Anisotropic Materials," *Journal of Composite Materials*, vol. 5, no. 1, pp. 58-80, 1971.
- [4] P. Alexis Castel, P. Sebastian Müller and A. Trameçon, "Fairing separation shock source evaluation and propagation," in *ECSSMET 2023*, Toulouse, France, 2023.